Identification of anisotropic properties of polymer sheets from heterogeneous biaxial tests

Hanane Attar, Yun-Mei Luo, Luc Chevalier, Thanh Tung Nguyen, Fabrice Detrez

Identification of anisotropic properties of polymer sheets from heterogeneous biaxial tests

Hanane Attar, Yun-Mei Luo, Luc Chevalier, Thanh Tung Nguyen, Fabrice Detrez*

Université Paris-Est, Laboratoire Modélisation et Simulation Multi Echelle, MSME UMR 8208 CNRS, 77454 Marne-la-Vallée, France

*corresponding author: yunmei.luo@univ-paris-est.fr

Abstract

The stretch blowing process for PET bottle induces the anisotropic mechanical properties due to the different elongation of macromolecular chains. For example, the Young's modulus can be multiplied by almost two in the longitudinal direction and more than 3 times in the hoop direction of the plastic bottle. However, the process is complex and the elastic properties present dispersions which depend on the process condition. Therefore, it is necessary that the 5 parameters from the orthotropic elastic properties can be all obtained during a single realization. The symmetry of the elasticity tensor reduces to 4 characteristics to be determined. To achieve this identification process, firstly, the displacement field is measured using image correlation and biaxial tests which are carried out on a machine developed in our laboratory. Then, the virtual field method on a specific cruciform specimen with a hole is managed to identify the orthotropic elastic properties. The optimal position of the hole is also studied. The identified orthotropic constitutive parameters from this method is compared to the results obtained by classical methods.

Keywords

Virtual field method, orthotropic elastic properties, heterogeneous biaxial test

Introduction: towards stochastic modelling of PET induced properties

Injection stretch blow moulding (ISBM) process [1-3] is a complex process that involves several stages from PET granular to the final bottle. Injected preforms are heated by infrared radiation so that temperature becomes higher than the glass transition of the material. The bottle is then obtained by biaxial elongation: longitudinally with a rod, in hoop direction by air under pressure. It is well known that mechanical properties of the PET [4-7], in particular the Young modulus of the material, increases during the process. This increase depends on many parameters as the initial morphology of the preform, the initial temperature profile before stretching, the elongation rate and the final elongation

[8-10]. Consequently, and even in industrial and steady conditions, the induced mechanical properties of the produced bottles are anisotropic.

Currently, manufacturers managed real tests on blown bottles: maximum pressure or critical loads can be measured and when values are strong enough, the design is validated. Being able to simulate accurately without forming the bottle would be a great help for ISBM industry. This subject has been addressed since a long time [1-3, 11-15] but always concluded to the necessity of the accurate knowledge of the induced mechanical properties as well as the thickness distribution that are needed to manage an accurate simulation. In case of bottles with a large cylindrical part, the assumption of an orthotropic behavior can be done and five parameters must be identified E_z, E_θ, $\upsilon_{\theta z}$, $\upsilon_{z\theta}$ and $G_{\theta z}$. with a symmetry relation between the four first. A classical way to manage identification is to cut three specimens from the bottle at 0°, 45° and 90° (see fig.1). Consequently, six information can be obtained and a least square method can achieve the identification.

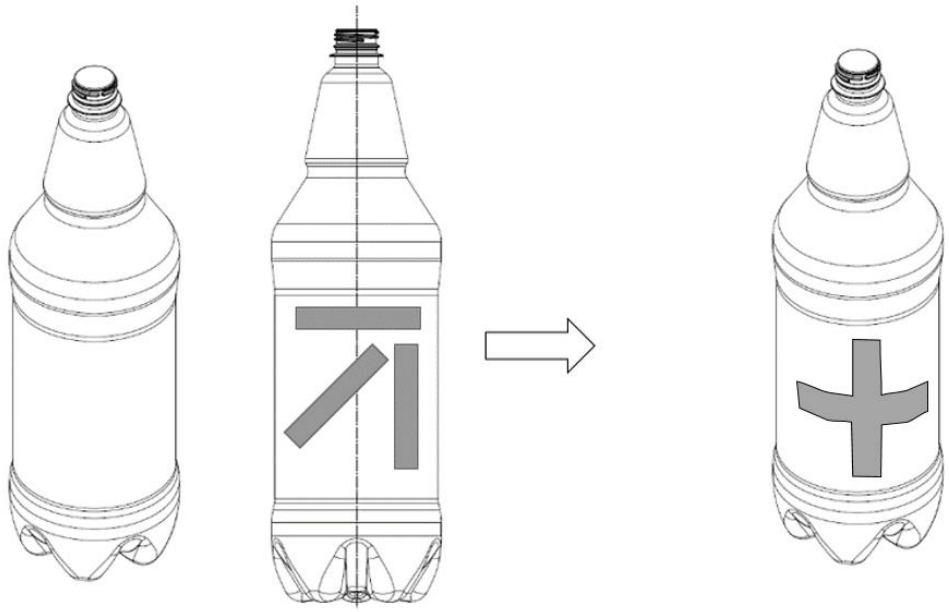

Figure 1: *Bottle shape and classical approach for identification from three uniaxial tensile specimen cut from directions 0, 90 and 45° (left) cross specimen for biaxial tensile test (right).*

In previous paper [16], authors have already presented methods for identification of the mechanical properties based on digital image correlation and virtual field (VFM) method [17]. Using a global blowing test, the 3D displacement field allows the determination of both Young modulus in orthotropic

directions but the homogeneity of the strain field does not allow the determination of Poisson's ratio or shear modulus. Using a heterogeneous uniaxial tensile tests managed on specimen cut in longitudinal or hoop direction, 2 Poisson's ratio are obtained directly and modulus can be evaluated, the heterogeneous tensile test can give at last, the shear modulus of the orthotropic behavior law. This identification process necessitates two steps and it can be shown that uniaxial tensile test cannot give all five parameters with only one test.

In this paper, a heterogeneous biaxial tensile test managed on cruciform specimen with hole is carried out. This experimental result combining with virtual field method allows us to obtain the orthotropic characteristics from a single biaxial test. The virtual field (VFM) method is applied on the heterogeneous tensile test. This method is wildly used for the identification of mechanical behavior of linear elastic materials [17-22]. In the recent past, the VFM method is applied for the identification of hyperelastic constitutive parameters [19] or viscoelastic properties of rubber under dynamic tests [20]. Pierron et al. identified the orthotropic elastic law under a macroscopic shear test named unnotched Iosipescu [21]. Marek et al. considered the virtual displacement fields which were proportional to the sensitivity of stress field to perform the identification of an anisotropic plasticity behavior [22].

In section 2, four virtual displacement fields are necessary for identification all parameters in orthotropic behavior law. Furthermore, in order to well consider the shear strain field, one of the virtual displacement fields is chosen on focus near the hole of our specimen. The position of hole on the specimen is studied in order to obtain the maximum accuracy for the five parameters. In section 3 we present the portable testing machine developed at our laboratory to carry out biaxial tensile test in different environment. Usually, the apparatuses in the literature are often complex and especially applying the load that lead to a homogeneous strain field [23-26]. A vertical biaxial testing machine has been built up at our Laboratory. The simple design of the machine consists of four independent actuators and load sensor is provided along each arm for the force measurement. The biaxial tensile test managed on cruciform specimen with a hole is performed. Digital image correlation [27-29] is used

to determine the heterogeneous strain field. Finally, the virtual field method is used for identification for all elastic orthotropic characteristics is discussed in section 4.

II. Theory: virtual field method applied on heterogeneous tensile biaxial test

Our purpose is to manage biaxial tensile test on "square" specimen. Using digital image correlation (DIC for short) we follow the displacement field on the entire surface of the specimen. Used together with the virtual filed method (VFM for short) one can identify the elastic properties.

II.1. Choice of virtual displacement field

Let us recall basics of the virtual field method (VFM for short). The virtual field principle writes:

$$\iint_{\partial\Omega} \overrightarrow{F_s}.\overrightarrow{u^*}dS = \int_{\Omega} \underline{\underline{\sigma}} : \underline{\underline{\varepsilon}}^* dV \quad \text{for all } \overrightarrow{u^*} \tag{1}$$

Ω is the studied domain of the specimen and $\partial\Omega$ is the boundary of the domain. $\underline{\underline{\sigma}}$ is the real stress tensor and $\underline{\underline{\varepsilon}}^*$ is the virtual strain tensor obtained from the virtual displacement $\overrightarrow{u^*}$. In case of an orthotropic material, the behavior law writes:

$$\underline{\underline{\sigma}} = \underline{\underline{\underline{\underline{K}}}}.\underline{\underline{\varepsilon}} \quad \text{or} \quad (\sigma) = [K].(\varepsilon) \text{ with, in 2D: } [K] = \begin{bmatrix} K_{xx} & K_{xy} & 0 \\ K_{xy} & K_{yy} & 0 \\ 0 & 0 & 2G_{xy} \end{bmatrix} \tag{2}$$

One must notice that $K_{xy} = \upsilon_{yx} K_{xx}$ or $K_{xy} = \upsilon_{yx} K_{yy}$ and consequently, if we manage an uniaxial tensile test in *X* direction on a rectangular specimen (length *L* × width *b* × thickness *e*) and if we use two simple virtual displacement fields as:

$$\overrightarrow{u_1^*} = x\vec{x} \Rightarrow \underline{\underline{\varepsilon}}_1^* = \begin{pmatrix} 1 & 0 \\ 0 & 0 \end{pmatrix} \text{ and } \overrightarrow{u_2^*} = y\vec{y} \Rightarrow \underline{\underline{\varepsilon}}_2^* = \begin{pmatrix} 0 & 0 \\ 0 & 1 \end{pmatrix} \tag{3}$$

Then the VFM leads to two relations:

$$\iint_{\partial\Omega} \overrightarrow{F_s}.\vec{x}.x ds = \int_{\Omega} \sigma_{xx} dS = \int_{\Omega} \left(K_{xx}\varepsilon_{xx} + K_{xy}\varepsilon_{yy} \right) dS \Rightarrow \boxed{\frac{FL}{V_\Omega} = K_{xx}\overline{\varepsilon_{xx}} + K_{xy}\overline{\varepsilon_{yy}}}$$
$$\iint_{\partial\Omega} \overrightarrow{F_s}.\vec{y}.y ds = \int_{\Omega} \sigma_{yy} dS = \int_{\Omega} \left(K_{xy}\varepsilon_{xx} + K_{yy}\varepsilon_{yy} \right) dS \Rightarrow \boxed{0 = K_{xy}\overline{\varepsilon_{xx}} + K_{yy}\overline{\varepsilon_{yy}}} \quad (4)$$

where $\bar{}$ is the operator of mean value: $\overline{\varepsilon_{xx}}$ and $\overline{\varepsilon_{yy}}$ are the mean values of strain ε_{xx} and ε_{yy} respectively, over the entire domain studied. V_Ω is the volume of the specimen (i.e. $V_\Omega = L \times b \times e$). Considering the previous remark on K_{ij} coefficient, these second equation can explicitly give the Poisson's ratio υ_{xy} whatever the real strain field is or is not homogeneous by the following:

$$\upsilon_{xy} = -\frac{\overline{\varepsilon_{yy}}}{\overline{\varepsilon_{xx}}} \quad (5)$$

However, this approach fails to give the two K_{xx} and K_{yy} parameters in case of orthotropic materials. A third virtual displacement field should be considered to provide a third equation which is independent from the two previous one. This is not possible from a homogeneous tensile test and remains quite difficult for heterogeneous strain field provided using a central hole in the specimen. Getting a fourth equation in order to identify all parameters on a single tensile test seems impossible.

In case of biaxial tensile test, one can take benefit of two load measures F_x and F_y and can provide an optimal shape for a given third virtual displacement field in order to identify all 5 parameters with a single test. We propose a square geometry for the specimen (side *a* x thickness *e*) with circular holes (radius *R*) at random positions. First, the best position of a unique hole is studied (Fig. 2). Using the same two virtual fields already presented in equation (3) leads to the two relations:

$$\frac{F_x a}{V_\Omega} = K_{xx}\overline{\varepsilon_{xx}} + K_{xy}\overline{\varepsilon_{yy}}$$
$$\frac{F_y a}{V_\Omega} = K_{xy}\overline{\varepsilon_{xx}} + K_{yy}\overline{\varepsilon_{yy}} \quad (6)$$

None of these two relations gives the Poisson's ratio anymore but it is easy to add a third virtual displacement field to complete the system of three equations for three parameters:

$$\overrightarrow{u_3}^* = x(x-a)\vec{x} + y(y-a)\vec{y} \Rightarrow \underline{\underline{\varepsilon}}_3^* = \begin{pmatrix} 2x-a & 0 \\ 0 & 2x-a \end{pmatrix} \quad (7)$$

In that case the displacement is naught on the edges of the specimen, so external loads do not appear any more. The mean values of the virtual strains ε^*_{xx} and ε^*_{yy} are naught on the specimen. Consequently, measured strains must be heterogeneous, but more, they must not be symmetric with respect of the square axis otherwise the products of (*2x-a*) or (*2y-a*) with ε_{xx} or ε_{yy} will be naught also. This can be obtained by fixing a hole in the specimen. In that case, the VFM gives this third relation:

$$K_{xx}\overline{(2x-a)\varepsilon_{xx}} + K_{xy}\overline{(2y-a)\varepsilon_{xx} + (2x-a)\varepsilon_{yy}} + K_{yy}\overline{(2y-a)\varepsilon_{yy}} = 0 \quad (8)$$

This last is independent of the two first relations and the trio K_{xx}, K_{yy} and K_{xy} can be determined.

The strain fields will make it possible to identify all modulus E_x, E_y and Poisson's ratio but the determination of G_{xy} may be difficult because of the small region where shear occurs near the hole. Considering the heterogenous shear strain field, in order to equilibrate the contribution of the two components ε_{xx} and ε_{yy} in regard of the component ε_{xy} we choose a fourth displacement field which will focus near the hole and that is define as:

$$\begin{aligned} \varepsilon_{xy}^* &= 1 \quad \text{if } 1 - \frac{(x-x_o)^2 + (y-y_o)^2}{d^2} \geq 0 \\ \varepsilon_{xy}^* &= 0 \quad \text{if } 1 - \frac{(x-x_o)^2 + (y-y_o)^2}{d^2} < 0 \end{aligned} \quad (9)$$

x_o and y_o are the coordinates of the center of the circular domain where we apply the VFM and *d* is the typical dimension of this region. In order to determine the ε_{xx}* and ε_{yy}* we must integrate this field, which leads to:

$$\left.\begin{aligned} u^* &= y \\ v^* &= x \end{aligned}\right| \quad \text{if } \varepsilon_{xy} > 0 \text{ and } u^* = v^* = 0 \quad \text{outside the domain} \quad (10)$$

It must be noted that the displacement field is discontinuous on the border of the selected area and high positive or negative values will appear on the circle that limit the area. Nevertheless, this displacement field can be used to obtain the fourth equation needed.

II.2. Optimization of the hole position

In the following, we present the numerical method followed to optimize the hole position defined by the coordinates of the center x_c and y_c.

II.2.1 Choice of the noise amplitude

First, one manages an orthotropic finite element simulation of the biaxial test with a hole randomly located in the specimen: we obtain a finite solution U_{FE}. Figure 2a shows the mesh and the imposed displacement on the edges. Using the VFM from this displacement field, one can perfectly identify the parameters used to manage the simulation: E_1=3000MPa, E_2=6000MPa, υ_{12}=0.2, υ_{21}=0.4. Second, we perturb this finite element solution by adding a random perturbation to simulate the experimental uncertainties:

$$U_{DIC} = U_{FE} + U_{\max}\left(rand - \frac{1}{2}\right)noise\% \tag{11}$$

where U_{max} is the maximal value of the displacement components, *rand* is a uniform random field varying from 0 to 1 and noise% is the percentage of U_{max} used to generate the experimental uncertainties. Because the perturbation is random, the identification necessitates 30 realizations for each noise percentage. The mean value of the parameter and the standard deviation are calculated and the graphs of Fig. 2b show the evolution of the mean parameter versus noise percentage in thick dark line and the mean value plus or minus standard deviation in grey line to characterize the dispersion of the identification.

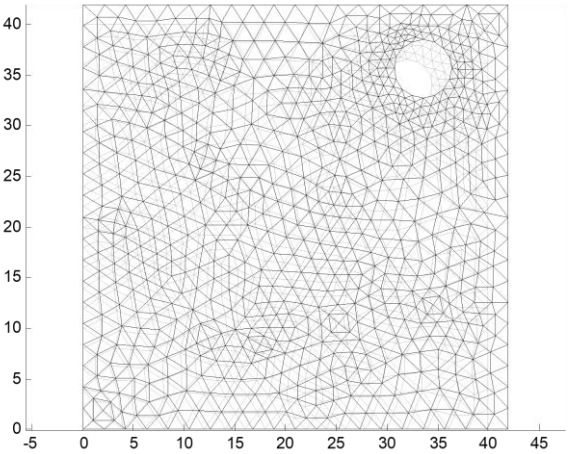

(a)

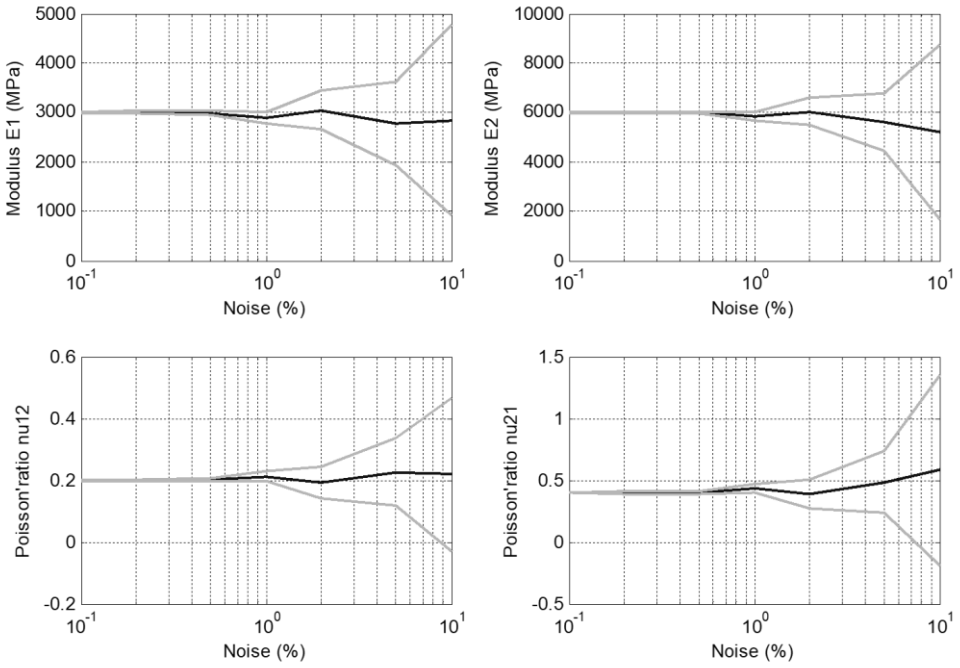

(b)

Figure 2: *Biaxial heterogeneous specimen: (a) initial and deformed mesh and (b) influence of noise percentage on identification accuracy.*

One can see from Fig.2 that the mean value remains acceptable even when noise reaches 10% but the dispersion on the 30 identifications increases quickly and is no more acceptable after 2% of random noise. In the following, we will use 2% noise to explore the best specimen geometry.

II.2.2 Optimization of hole position from Monte Carlo method

The best position x_c and y_c for the center of the hole is necessary to carry out. To manage this investigation we reproduced the same procedure than previously but instead of varying the noise

percentage, we fixed 2% and varied the x_c and y_c coordinates. We already said that the strain field ε_{xx} and ε_{yy} should not present symmetry and surely, placing the hole at the square center is definitely a bad idea with the third virtual displacement we choose.

On Fig. 3 we plot the mean value of the parameter (black spot) and the mean value plus or minus the standard deviation of the parameter (grey spot). Each spot is located at the x_c, y_c location of the hole. 1000 realizations of the hole location have been managed and looking at the clouds of spots, a specific point of view highlights a "valley" where dispersion is very high and parameter values badly estimated. This "forbidden valley" can be characterized by the equation y_c=-1.23 x_c+44.60. One can see that the center of the square specimen, $x_c = y_c = 20mm$, is on this line but it is not the only forbidden location.

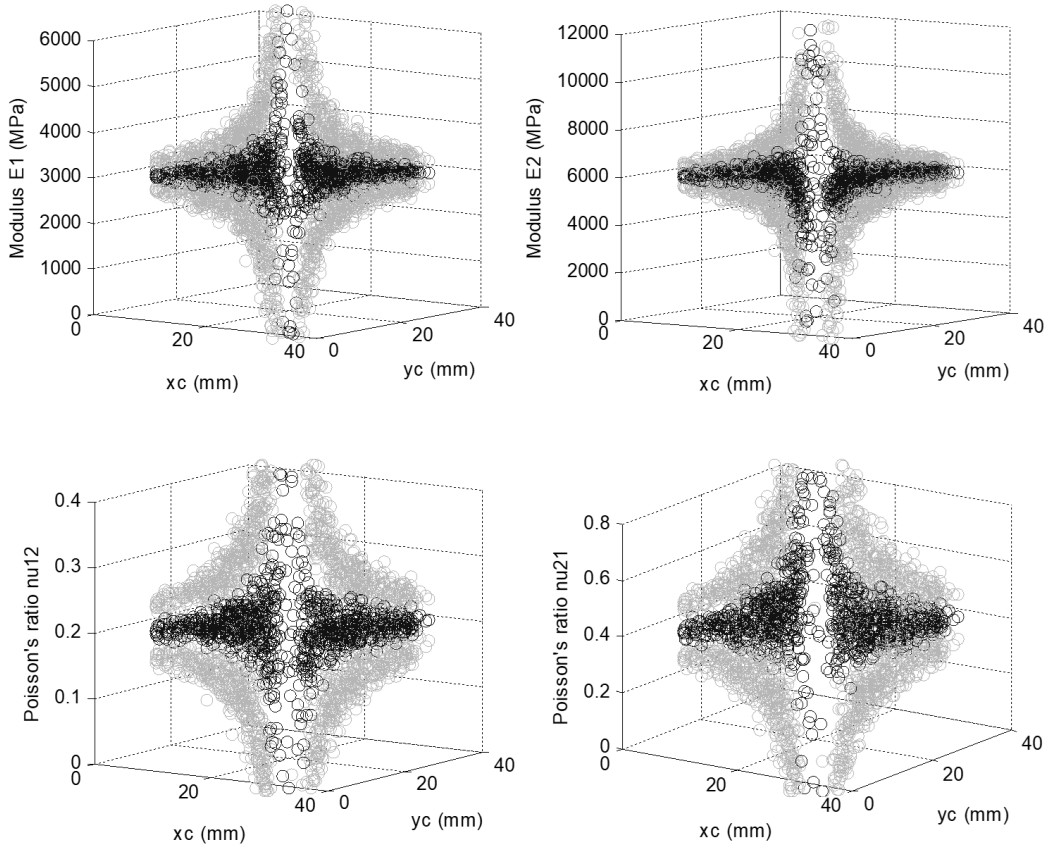

Figure 3: *Biaxial heterogeneous specimen with one hole: uncertainties versus the hole location x_c and y_c.*

These forbidden positions for the hole lead to a hill posed problem. The location is almost on a diagonal of the square specimen because of the anisotropy of the material. For the chosen virtual field, equation (8) gives:

$$\overline{(2x-a)\sigma_{xx}} + \overline{(2y-a)\sigma_{yy}} = 0 \qquad (12)$$

Equi-biaxial displacements are imposed on the edge of the square, consequently, the strains ε_{xx} and ε_{yy} have identical distribution around the hole but stresses σ_{yy} are certainly higher than σ_{xx} because E_1 is lower than E_2. In the upper left corner as well as in the lower right corner of the square, the two expressions (2x-a) and (2y-a) have opposite signs and the two terms of the Eq.12 can be opposite. This leads to 0=0 and cannot provide the determination of the three parameters.

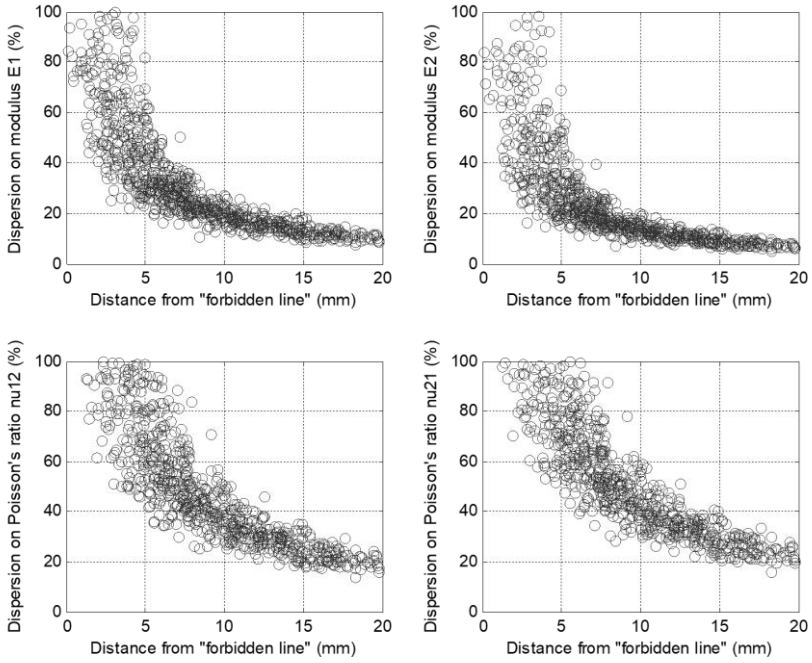

Figure 4: *Dispersion on the 30 realizations of the identification for a given hole versus the distance between the hole's center and the "forbidden line".*

Considering the decreasing shape of the dispersion when the center of the hole is far from the "forbidden valley", one can suggest that a good criteria for an accurate identification is the distance between the center of the hole and the line characterized above. Plotting the dispersion versus this distance d_C shows a nice decreasing evolution (see Fig.4).

III. Biaxial tensile tests on heterogeneous specimen

In this section, we present the development and design of the biaxial testing machine and biaxial heterogeneous tests managed for the identification problem. The design of the machine is presented and also the test procedure and typical results and specifications of the test campaign.

III.1. Biaxial test apparatus developed at MSME lab

The tests are carried out from a home made biaxial tensile machine (*Fig. 6*). This tensile device has been developed under several criteria: (i) it must allow the polymers to be stretched in two directions with large strain, with high strain rate and regulated temperature; (ii) the size must remain small enough to be easily transportable in order to manage *in situ* biaxial test under X-ray synchrotron facilities. As complementary equipment, a High-Speed camera to capture images during stretching is needed for DIC, a heating system must be adapted and a "free" zone allowing the passage of the X-ray beams to reach the material needs to be managed. The system is modular and consists of four drives (CMMP-AS-C5-11A-P3-M0) which control four motors (EMMS-AS-100-M-HS-RMB) each connected to an electrical actuators (ESBF-BS-63- 100 -10P) from FESTO. The actuators have a maximum speed of 530 mm/s and a stroke length of 100 mm. At the end of each actuators, force sensors are installed. These sensors are connected to clamps which allow the studied sample to be held. They have a nominal force of 10kN.The four actuators are piloted independently with the programming software LABVIEW via the Modbus TCP/IP protocol. This software is used to control the actuators but also to provide data acquisition on the force measured by the sensors. The four independent actuators are controlled to ensure that the specimen center remains motionless or stationary.

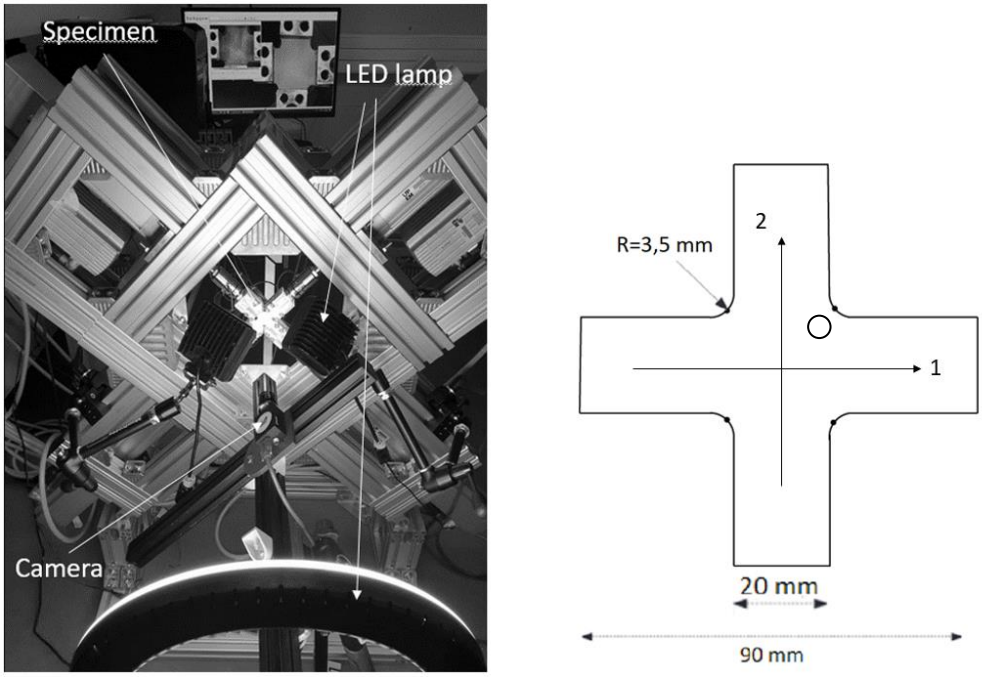

Figure 5: *Biaxial testing machine and specimen (for the experimental section, 1 is the longitudinal direction and 2 the circumferential direction of the bottle).*

A camera located in front of the sample allows image capture during material deformation. We use the VIC2D software which enables image correlation to determine the displacement and deformation fields. In the present study, an equibiaxial test was performed on a cross specimen (Fig. 5) cut from PET bottles. Direction 1 is the circumferential direction of the bottle and direction 2 is the longitudinal direction.

The precise shape is obtained with a water jet cutting machine. The displacement of the four actuators are equal and were set at 0.02mm steps with a 0.001mm/sec speed. Images of the surface of the specimen at increasing stretches were stored at each displacement of 0.02mm per direction.

III.2. Tensile specimen and biaxial tests

The displacement field at the surface of the sample was determined using the DIC technique. It consists in making the grey levels correspond between two different images of a given area, each image corresponding to different levels of deformation. In order to improve the contrast of the image, we must first paint the sample white and cover it with a black spot. This leads to a random grey field. Uniform illumination of the sample surface is provided by LED lamp. The camera is fixed on an

adjustable support. The VIC-2D software is then used for the correlation process. The software processes the images and allows us to obtain the displacement distribution.

As shown in Fig.5, to avoid the stress singularities at the corner of a square specimen, the real geometry is cut with quarter of circles at each corner. This specific shape generates heterogeneities that could be enough to identify all the parameters. This difference with the square geometry used in the previous section slightly modifies the slope of the forbidden line (Fig.6).

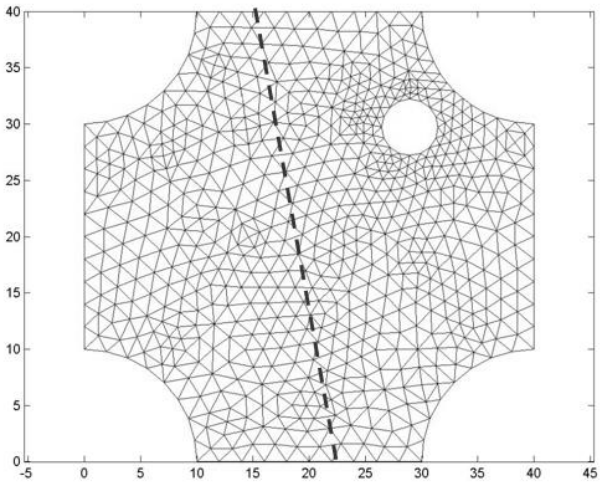

Figure 6: *Best specimen with one hole. The forbidden line has a higher slope than the square specimen for the same anisotropy.*

Figure 7: *(a) Biaxial specimen with hole and speckle cut from bottle with water jet machine; (b) placed on biaxial machine with speckle.*

As explained previously, the symmetry makes it difficult to choose four different virtual displacement fields that lead to independent equations. Consequently, we provide a hole to break this symmetry and the hole is managed in the top right region of the specimen as shown on Fig. 7. We neglect the effect of the curvature of the bottle and make the 2D plane stress assumption for this test. The material is supposed to be homogeneous within the thickness and the axis of anisotropy are aligned with *X* and *Y* directions.

Because of the orientation of the specimen chosen for the experimental study, the forbidden line goes from the left bottom to the top right. That is a consequence of the higher value of the circumferential modulus compared to the longitudinal one.

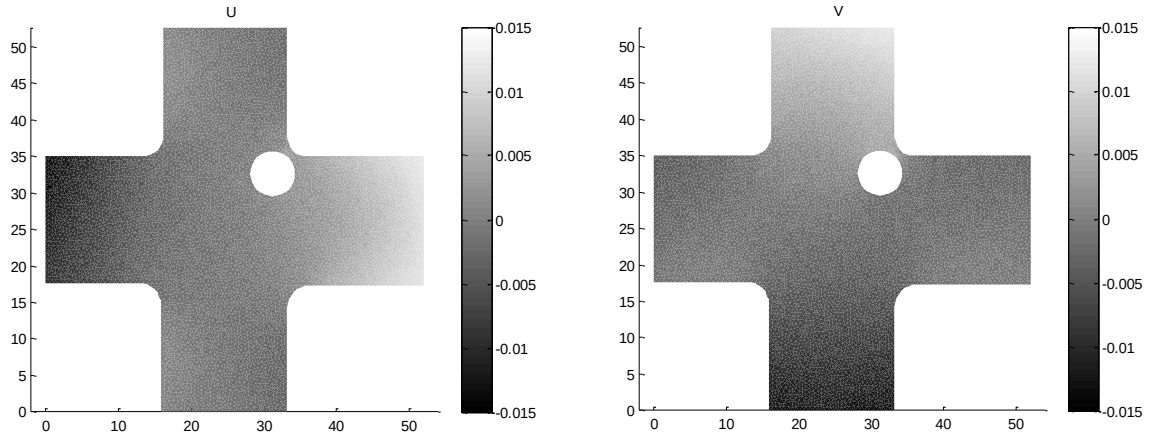

Figure 8: *Biaxial displacement field from VIC-2D (a) horizontal displacement U and (b) vertical displacement V.*

Figure 8 shows typical displacement field components, the center of the specimen has *U* and *V* components equal to 0 and one can see that *U* is negative at the left and positive on the right side in the two horizontal arms while it is in the bottom arm that *V* is negative and the top arm is positive. Considering the irregularities in the *U* and V fields, one can estimate the noise is less than 1%. This is less than the noise level considered in the theory section.

This displacement field is typical of a biaxial stretching but one can see that contours of both components become irregular near the hole that generates shear and breaks the symmetry. So, it is

also possible to propose a fourth virtual displacement field in order to identify the shear modulus G_{xy} and complete the in-plane characteristics of the material.

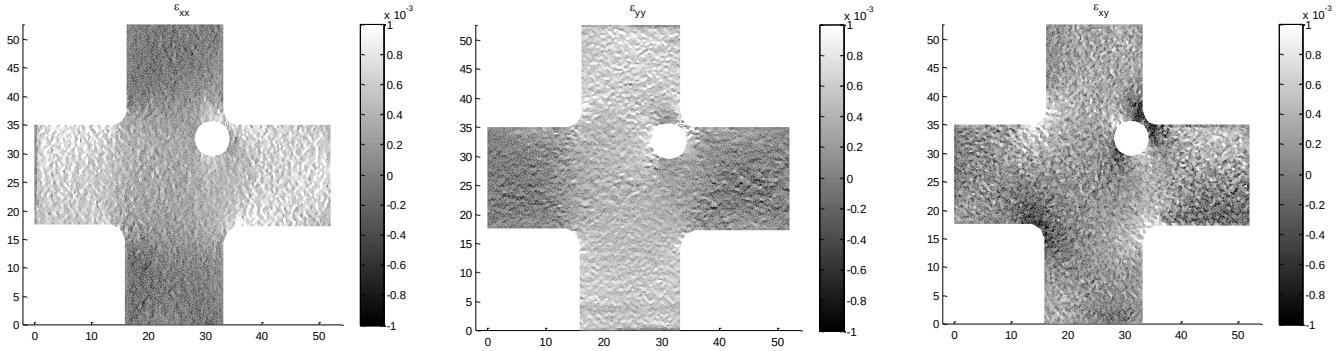

Figure 9: *Biaxial strain field from VIC-2D.*

IV. Results and discussion

IV.1. Results

Forty biaxial tests were carried out in order to identify accurately the material parameters. Young's modulus, Poisson ratios and shear modulus are summarized in Fig.10. Mean values of the parameters are given in Table 1 and one can see that the longitudinal modulus E_z = 3250MPa, is almost half of the circumferential one E_θ. Inverse proportion are measured for the corresponding Poisson ratios.

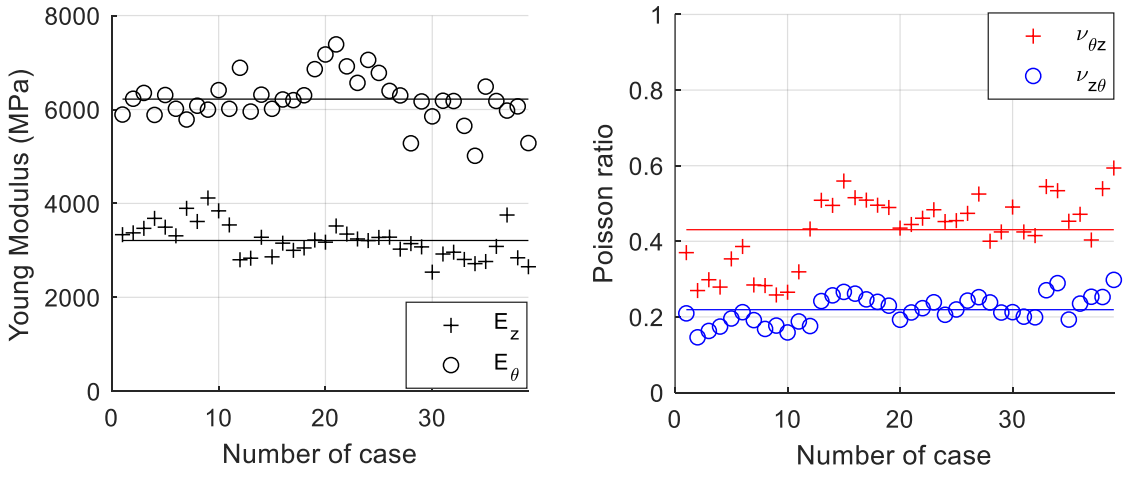

(a) (b)

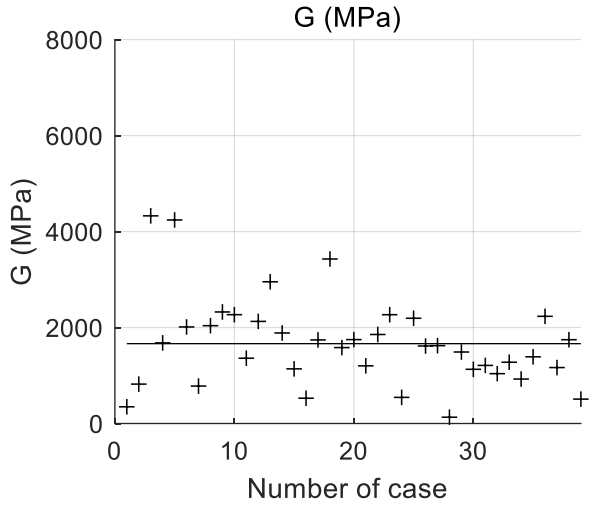

Figure 10: *(a) Young Modulus; (b) Poisson ratios; (c) Shear modulus*

The dispersions from one sample to another for parameters E_z, E_θ, $\nu_{\theta z}$, $\nu_{z\theta}$ and $G_{z\theta}$ are respectively: 8%, 12%, 24%, 18% and 55%. This last is very important and will be discussed in a following subsection.

IV.2. Discussion on modulus and Poisson ratios

The dispersion on E_z is lower than the one on E_θ: this has already been notice in [16]. The reason is that the strain rate in the longitudinal direction, during the ISBM industrial process, is given by the elongation rod. Its speed is more regular than the effect of the air pressure on the hoop strain rate. Consequently, the induced longitudinal modulus variation from bottle to another are smaller.

Table 1 also gives the mean values of these two modulus measured from different methods. In method 1, we conduct the classical approach cutting three specimen at 0°, 45° and 90° from the bottle to provide uniaxial tensile tests. Method 2 is presented in [16]. In this method, firstly, one of the Poisson's ratios is identified from an uniaxial tensile test on a plane specimen with a hole. Then, the modulus are measured using a 3D digital image correlation from bottles blown with internal pressure. These two steps give E_z, E_θ, $\nu_{\theta z}$ and $\nu_{z\theta}$. Finally, back on the tensile test with the hole, one can evaluate the shear modulus from the heterogeneity around the hole. Comparing the mean values of the modulus E_z and E_θ one can see that our method provides results that are between method 1 and 2. This is also the case for Poisson's ratio. The parameters of our method are identical to the values identified by classical methods: differences between methods are lower than the dispersion of each method. For example, the max difference on E_z is 4.7% when dispersion between samples in our method is 8%.

Table 1 Comparison of orthotropic properties from different method

	E_z (MPa)	E_θ (MPa)	$\nu_{\theta z}$	$\nu_{z\theta}$	$G_{z\theta}$ (MPa)
Method 1	3150	5900	0.41	0.22	1250
Method 2	3480	6340	0.42	0.23	1500
Our method	3250	6200	0.42	0.22	1660

IV.3. Discussion on the shear modulus

Considering the particular case of the shear modulus, one can notice that its value varies from one method to another (32% difference between Method 1 and our method). The shear modulus also highlights a very large dispersion (up to 55%) in our method. This is certainly due to the combination of two reasons.

First, a material reason: the shear stiffness is strongly related to the way that the macromolecular chains of PET stretch in longitudinal and hoop directions to generate a kind of rectangular network. The microstructure could be modelled as a long fiber braided orthotropic material where the shear modulus depends on the friction between fibers and the properties of the bulk. More, the elongation is not so well reproduced in the hoop direction and finally, it leads to large dispersion on the shear behavior.

Second, the method impact: the area where shear occurs is small (around the hole and in corner) and the DIC measure does not provide enough data to reduce the experimental uncertainties. One must work to improve this specific problem.

Nevertheless, this method enables the determination of the complete set of elastic parameters of and supposed orthotropic material and numerous tests can lead to validation of recent stochastic modelling of elastic tensor [30-31].

V. Conclusions

In this work, we present a method to identify the entire in-plane properties of an orthotropic elastic model from a unique test conducted on a biaxial tensile testing machine. This is necessary, in case of dispersion of the material properties, if one wants to build a stochastic elastic tensor taking into account the correlated parameter.

To achieve this approach, heterogeneous biaxial tensile tests were managed on cruciform specimen with a hole. The cruciform specimens are cut from the cylindrical part of PET bottles in a region that is assume to be orthotropic. To reinforce the heterogeneity and break the symmetry, a hole is done on the specimen.

The location of the hole has been chosen from a numerical analysis of the sensibility of the identification versus the position of the hole. The virtual field method was applied to proceed the identification of the orthotropic mechanical properties, the conditioning of the system was discussed and the hole position optimized by the Monte Carlo method.

Forty biaxial tests were carried out to quantify the dispersion on the material parameters. The choice of the three first virtual displacement fields lead to a well-conditioned system that allows identification of the elastic properties of bottles similar as previous author's work [16]. By comparing the identified values with more classical approaches, this method with a single test provides the same values for each parameter: difference between the approaches is lower than the dispersion of each approach. This validates the method.

The choice of the fourth virtual displacement field needed to identify the shear modulus is specific because of the small area where shear occurs for such test. On original form located in the region around was chosen and validated by comparison with shear modulus values identified from tension tests with a sample cut at 45° of the orthotropic directions. Considering the important dispersion on this modulus, there is a good agreement between both methods.

In the future work, since all the induced mechanical properties exhibit some dispersion, a probabilistic description of the orthotropic behavior law will be studied. Because all parameters are identified from the same sample, it is possible to study if they are or not correlated as some theoretical works show.

Acknowledgement

Authors thank the Sidel group at France for providing the bottles and for financially supporting this work.

References

[1] Schmidt F. M., Agassant J. F. and Bellet M. Experimental study and numerical simulation of the injection stretch/blow moulding process, Polymer Engineering & Science, vol. 38, no. 9, 1399-1412, Sept 1998.

[2] Billon N., Erner A. and Gorlier E. Kinematics of stretch blow moulding and plug assisted thermoforming of polymers; experimental study, PPS-21, 2005.

[3] Nagarjappa C. C. PhD. Thesis, Developing and validating stretch blow moulding simulation through free blow experiments, Queens University Belfast, School of Mechanical & Aerospace Engineering, 2012.

[4] Nixon J., Menary G.H., Yan S. Finite element simulations of stretch-blow moulding with experimental validation over a broad process window. Int J Mater Form, Volume 10, Issue 5, pp 793–809, October 2017.

[5] Menary G.H., Tan C.W., Harkin-Jones E.M.A., Armstrong C.G., Martin P.J.. Biaxial Deformation of PET at Conditions Applicable to the Stretch Blow Molding Process. Polymer Engineering & Science, vol. 52, no3, pp. 671-688, 2012.

[6] Chevalier L., Luo Y. M., Monteiro E., and MenaryG. On visco-elastic modelling of polyethylene terephthalate behaviour during multiaxial elongations slightly over the glass transition temperature. Mechanics of Materials, vol.52, pp.103-116, 2012.

[7] Marco Y. Caractérisation Multi-Axiale du Comportement et de la Micro-Structure d'un Semi-Cristallin: Application au Cas du P.E.T..PhD Thesis, ENS Cachan, Cachan, 2003.

[8] Luo Y.M., Chevalier L. On Induced Properties and Self Heating during Free Blowing of PET Preform. International Polymer Processing, Vol. 34, No 3. P 330–338, 2019.

[9] Lebaudy Ph., Saiter J.M., Grenet J., Vautier C. Temperature distribution in poly(ethylene terephthalate) plate undergoing heat treatment. Diffusion influence and application, Polymer, Vol 36, Iss 6, p 1217–1221,1995.

[10] Monteix S., Schmidt F., Le Maoult Y. Experimental study and numerical simulation of preform or sheet exposed to infrared radiative heating. Journal of Materials Processing Technology 119(1-3), p 90-97. 2001.

[11] Michaeli W. and PapstW.. FE-Analysis of the Two-Step Stretch Blow Molding Process. SPE ANTEC Technical Papers 30 , Chicago, USA, 2004.

[12] Martin L., Stracovsky D., Laroche D., Bardetti A., Ben-Yedder R., and Di Raddo R. Modeling and Experimental Validation of the Stretch Blow Molding of PET. in SPE ANTEC Technical Papers, New York, 1999.

[13] Schmidt F. M., Agassant J. F. and Bellet M.. Experimental study and numerical simulation of the injection stretch/blow moulding process, Polymer Engineering & Science, vol. 38, no. 9, 1399-1412, Sept 1998.

[14] Menary G. H., Tan C. W., Picard M., Billon N., Armstrong C.G., Harkin-Jones E. M. A.. Numerical simulation of Injection stretch blow moulding: comparison with experimental free blow trials, 10th ESAFORM Conference on Material Forming, AIPConf. Proc, vol. 907, pp. 939-944, 2007.

[15] Chevalier, L., Linhone C., Regnier G..Induced crystallinity during stretch-blow moulding process and its influence on mechanical strength of poly(ethylene terephthalate) bottles, Plastics rubber and composites 28, 8, 393-401, 1999.

[16] T.T. Nguyen, Y.M. Luo, L. Chevalier, F. Lesueur. Stochastic simulation of top load test on poly(ethylene terephthalate) bottles: An experimental study on dispersion of elastic properties. Journal of Applied Polymer Science, Wiley, 2021, pp.50837

[17] M. Grédiac, Comptes rendus de l'Académie des sciences. Série 2, Mécanique, Physique, Chimie, Sciences de l'univers, Sciences de la Terre, 1989,309(1), 1.

[18] Pierron, F., Grediac, M.. The Virtual Fields Method: Extracting Constitutive Mechanical Parameters From Full- Field Deformation Measurements, Springer Science and Business Media, Berlin, 2012.

[19] A. Tayeb, J.-B. Le Cam, M. Grédiac, E. Toussaint, F. Canevet, E. Robin, X. Balandraud. Identification of Constitutive Parameters Governing the Hyperelastic Response of Rubber by Using Full-field Measurement and the Virtual Fields Method. SEM Annual conference, Jun 2019, Reno, United States. ff10.1007/978-3-030-30098-2_9ff. ffhal-02172548f.

[20] Yoon, Sh., Winters, M. & Siviour, C.R. High Strain-Rate Tensile Characterization of EPDM Rubber Using Non-equilibrium Loading and the Virtual Fields Method. *Exp Mech* **56,** 25–35 (2016). https://doi.org/10.1007/s11340-015-0068-3.

[21] Pierron, F., Vert, G., Burguete, R.L., Avril, S., Rotinat, R., & Wisnom, M.R. (2007). Identification of the Orthotropic Elastic Stiffnesses of Composites with the Virtual Fields Method: Sensitivity Study and Experimental Validation. *Strain, 43*, 250-259.

[22] Marek, A., Davis, F.M., Rossi, M. *et al.* Extension of the sensitivity-based virtual fields to large deformation anisotropic plasticity. *Int. J. Mater. Form.***12,** 457–476 (2019). https://doi.org/10.1007/s12289-018-1428-1.

[23] Shi, T., Hu, J., Chen, W., &Gao, C. (2020). Biaxial tensile behavior and strength of architectural fabric membranes. *Polymer Testing*, *82*, 106230.

[24] Kodaira, Y., Miura, T., Takano, Y., &Yonezu, A. (2022). Development of biaxial tensile testing for porous polymer membranes. *Polymer Testing*, *106*, 107440.

[25] E. Gorlier, J.F. Agassant, J.M. Haudin, N. Billon. Experimental and theoretical study of uniaxial deformation of amorphous poly(ethylene terephthalate) above glass transition temperature. Plast. Rubber Compos., 30 (2001), pp. 48-55.

[26] G.H. Menary, C.G. Armstrong, R.J. Crawford, and J.P. McEvoy, Biaxial deformation and experimental study of PET at conditions applicable to stretch blow molding. Rubber and Composites Processing and Applications, 29, 360-370 (2012).

[27] Jerabek, M., Major, Z., & Lang, R. W. (2010). Strain determination of polymeric materials using digital image correlation. *Polymer Testing*, *29*(3), 407-416.

[28] Grytten, F., Daiyan, H., Polanco-Loria, M., & Dumoulin, S. (2009). Use of digital image correlation to measure large-strain tensile properties of ductile thermoplastics. *Polymer Testing*, *28*(6), 653-660.

[29] Chevalier, L., Eddhahak A., Maalej Y. Concentration de contrainte : différentes techniques de mesure. Technologie, 133-08, 134-10, 2004.

[30] J. Guilleminot and C. Soize. Generalized stochastic approach for constitutive equation in linear elasticity: a random matrix model. International Journal for Numerical Methods in Engineering, 90(5):613–635, 2012. ISSN 1097-0207, 2012.

[31] J. Guilleminot and C. Soize. On the Statistical Dependence for the Components of Random Elasticity Tensors Exhibiting Material Symmetry Properties. Journal of Elasticity, 111(2):109–130, 2013. ISSN 1573-2681, 2013.